The Electric Organ Discharges of the Gymnotiform Fishes: I. *Apteronotus leptorhynchus*

Brian Rasnow and James M. Bower

Division of Biology, California Institute of Technology, 216-76, Pasadena, CA 91125 USA

Summary. We present high temporal and spatial resolution maps in 3-dimensions of the electric field vector generated by the weakly electric fish, *Apteronotus leptorhynchus*. The waveforms and harmonic composition of the electric organ discharge (EOD) are variable around the fish but highly stable over long times at any position. We examine the role of harmonics on the temporal and spatial characteristics of the EOD, such as the slew rate and rostral-to-caudal propagation. We also explore the radial symmetry of the fish's field. There are major differences in the direction of the electric field vector at the head and caudal body. In the caudal part of the fish, the electric field vector rotates during the EOD cycle. However, rostral of the pectoral fin, the field magnitude and sign oscillate while maintaining relatively constant orientation. We discuss possible functional ramifications of these electric field patterns to electrolocation, communication, and electrogenesis.

Key words: Electric organ discharge – EOD – Weakly electric fish – Electroreception – Electrolocation – *Apteronotus leptorhynchus*

Introduction

Weakly electric fish of the genus *Apteronotus* generate a weak, high frequency electric field (<100 mV/cm, 0.5-10 kHz) which permeates their local environment (Bullock and Heiligenberg 1986). These fish are acutely sensitive to perturbations in the electric field from nearby objects whose impedance is different from the surrounding water. To understand the operating principles of high frequency electric sense, we have been studying by measurement (Rasnow et al. 1993) and simulation (Assad et al. 1993; Rasnow et al. 1989) the fish's self-generated electric potential and field. In a previous study (Rasnow et al. 1993), we mapped the electric potential on the skin and midplane, which revealed complex spatial and temporal patterns in the electric organ discharge (EOD). In this paper, we present the electric field vector, measured in 3-dimensions near a fish.

Although the electric field and potential are mathematically related (the field is just the negative gradient of the potential), each highlights different aspects of the EOD. The electric field, $\mathbf{E}$, is related to the current density vector, $\mathbf{J}$, by Ohm's law: $\mathbf{E} = \rho\mathbf{J}$, where ρ is the local resistivity. Therefore, in the water, the electric field and current density are directly proportional and in phase with each other ($\rho = 5$ kΩ-cm in these experiments). The electric field has a unique value, whereas the potential value depends on the choice of reference. The electric field is also a better indicator of electrolocation sensitivity than is the corresponding potential. The perturbation of the field at the skin or the electric image due to a nearby object is proportional to the unperturbed electric field at the object (Rasnow 1996). The relationship between an object perturbation and the unperturbed electric potential is not as direct or simple.

Previous studies have measured the potential and/or a single component of the field approximately normal to the skin at various places around electric fish (e.g., Knudsen 1975; Hoshimiya et al. 1980). However, recent evidence suggests that some electroreceptors may also respond to tangential field components (McKibben et al. 1993; Yager & Hopkins, 1993). Furthermore, objects and other nearby fish may be affected by all field components, and not just the component normal to the skin (Rasnow 1996). We have therefore measured the 3-dimensional electric field vector instead of a single component or projection. Although it is more difficult to measure and visualize a vector quantity, it is also more revealing. Furthermore, the field vector obeys physical and mathematical constraints (such as Maxwell's Equations) which the components independently do not. These constraints serve as an independent verification of the measurements, and contribute to a physically complete and coherent picture of the EOD.

The present study confirms and elaborates on the EODs extraordinary temporal stability, variable harmonic composition, propagation, and other stereotypical features described previously (Rasnow et al. 1993; Hoshimiya et al. 1980; Bastian 1981). In addition, we systematically examine how these and other parameters vary on and around a fish. The resulting high resolution maps of the potential and field reveal several novel aspects of the electric organ discharge, including major differences between the rostral and caudal fields. In a companion paper (Rasnow 1996), we examine how small objects perturb the field and may be detected by the fish.

Materials and Methods

The experimental materials and methods are similar to those described in Rasnow et al. (1993). We present here just the differences. Additional details of the apparatus and protocol are presented in Rasnow (1994).

Subjects. We mapped the electric field of three *A. leptorhynchus* and two *A. albifrons*. Before recording, each fish was paralyzed with intramuscular injections of 10 to 25 μl Flaxedil (gallamine triethiodide), and occasional supplemental injections (e.g., 5 μl after 3 hours). The fish were centered in a 60 x 60 cm tank 18 cm deep. The mapping plane was oriented parallel to the water surface. All the data presented here are from one 21 cm female *A. leptorhynchus* taken during a contiguous 6 hour period. Comparisons with the other fish are discussed.

Electrodes. An array of four electrodes measured the electric field components around each fish. Each electrode was made from a 25 μm diameter silver wire whose tip was melted into a 150-250 μm diameter ball. The wire was insulated and held rigid in a 1 mm OD glass pipette with a long slender tip created in an electrophysiology electrode puller. Four such electrodes were glued together so their tips defined approximately three Cartesian axes with 1-2 mm separation (photographed in Rasnow et al. 1993, Fig. 1B). Rather than attempting to construct the array to extreme precision, the actual electrode positions deviated slightly from this plan, and were calibrated before the experiments (see below). With 4 electrodes in such close proximity, care was taken to keep each electrode support structure small and electrically "transparent" to the adjacent electrodes. The glass insulation near the tip was thin and the shanks further away were glued with numerous holes and gaps between each other. The electrodes had impedances of approximately 40 kΩ, dominated by spreading resistance of the water (Robinson 1968; $R_S = \rho/4\pi r_e$, where ρ = water resistivity = 5 kΩ-cm, and r_e = electrode radius $\approx$ 100 μm). Three larger (and lower impedance) stationary electrodes were mounted on the tank walls.

Electrical instrumentation, Each of the seven electrodes was connected to a separate high impedance (>50 MΩ) follower amplifier mounted near the array. The follower outputs went to five wide bandwidth (10 Hz to 60 kHz; -3 dB) differential amplifiers, which in turn were connected to five 16-bit delta-sigma analog-to-digital converters (ADCs). Three channels provided potential differences from the array, from which the electric field vector was computed (the left side of Eqn. 1, below). The fourth channel recorded the potential between the array and a distant stationary electrode lateral of the fish. The fifth channel served as a phase reference, recording the potential between stationary electrodes located rostral and caudal of the fish. The ADCs sampled synchronously at 48,000 samples/second/channel. They also digitally low-pass filtered the EOD without aliasing or phase distortion (±0.001dB below 22 kHz, –86 dB above 26 kHz; Welland et al. 1989). System noise was approximately 1.6 μVRMS over a 10 kHz bandwidth, on the order of the Johnson noise of the electrodes (Horowitz and Hill 1989; Rasnow 1994).

Electrode positioning. The electrode array and follower amplifiers were mounted on a small platform above the fish tank. The platform position was controlled either manually or by computer. The array could be rapidly positioned closer than 1 mm from the fish, and the precise positions were recorded with a computer-video overlay system (Rasnow 1994).

Computing electric field vectors, Although the electric field can, in principle, be computed from a numerical gradient of potential measurements, in practice this amplifies noise and measurement errors. The numerical gradient is a small difference of two large potentials, and is also extremely sensitive to positional errors in the measurements. We avoided these problems by using a rigid electrode array and differential recording between electrode pairs.

When the electrode array is in a field, $\mathbf{E} = (E_x, E_y, E_z)$, averaged over the volume of the array, the measured potential differences between electrodes are proportional to the field and the interelectrode distances:

$$\begin{bmatrix} \varphi_2 - \varphi_1 \\ \varphi_3 - \varphi_1 \\ \varphi_4 - \varphi_1 \end{bmatrix} = \begin{bmatrix} x_2 - x_1 & y_2 - y_1 & z_2 - z_1 \\ x_3 - x_1 & y_3 - y_1 & z_3 - z_1 \\ x_4 - x_1 & y_4 - y_1 & z_4 - z_1 \end{bmatrix} \begin{bmatrix} E_x \\ E_y \\ E_z \end{bmatrix} \quad (1)$$

where electrode k, at position (x_k, y_k, z_k) is at potential φ_k. The electric field components were computed from the potential differences by inverting Eqn 1. The accuracy of the field components is related directly to the accuracy with which the interelectrode spacings, of order 1–2 mm, can be determined. If the array were perfectly orthogonal, then the matrix in Eqn. 1 would be diagonal, and each electric field component would be proportional to the potential difference between a single electrode pair. However, the array was only approximately orthogonal. Thus the pairwise measured potential differences consisted of linear combinations of the electric field components, which had to be resolved.

Calibrating interelectrode distances. It is difficult to accurately determine interelectrode distances optically. The electrodes are not perfectly spherical so estimating their center is somewhat judgmental. Furthermore, the orientation of the array under a microscope must precisely match the orientation in the fish tank. We therefore developed the following method for determining effective interelectrode distances *in situ*, by placing the array in a known electric field and measuring a large set of potential differences. The differences between measured and theoretical data were minimized by varying the electrode positions using two successive Nelder-Meade simplex optimizations (Dennis and Woods 1987). A dipole, made of two ball bearings connected to a function generator, was placed in the recording tank. The potential, measured relative to an electrode on the tank wall near the dipole zero-potential plane, and the potential differences between pairs of electrodes in the array, were measured as the array moved along several paths, lateral, perpendicular, and above the dipole. (Fig. 1A) The theoretical potential at a point $\mathbf{x}$ (in an infinite tank) is:

$$V(\mathbf{x}) = \frac{\rho I}{4\pi}\left(\frac{1}{|\mathbf{x} - \mathbf{x}_1|} - \frac{1}{|\mathbf{x} - \mathbf{x}_2|} \right) \quad (2)$$

where I is the current supplied by the function generator, ρ = 5kΩ-cm is the water resistivity, and $\mathbf{x}_1$, $\mathbf{x}_2$ are the position vectors of the two poles. Because of the large tank size (60x60x18 cm) relative to the dipole separation (approximately 4 cm), the side walls had negligible effect near the poles, however the tank floor and water surface confined the field. These surfaces were accounted for analytically using the method of images (Jackson 1975).

The first optimization made small adjustments to the visually estimated pole positions $\mathbf{x}_1$ and $\mathbf{x}_2$ by minimizing the

difference between measured and computed potential (relative to the wall).

The second optimization computed the inverse of the interelectrode distance matrix, by minimizing the difference between the field components computed from the differential measurements, and the theoretical electric field of a discrete dipole:

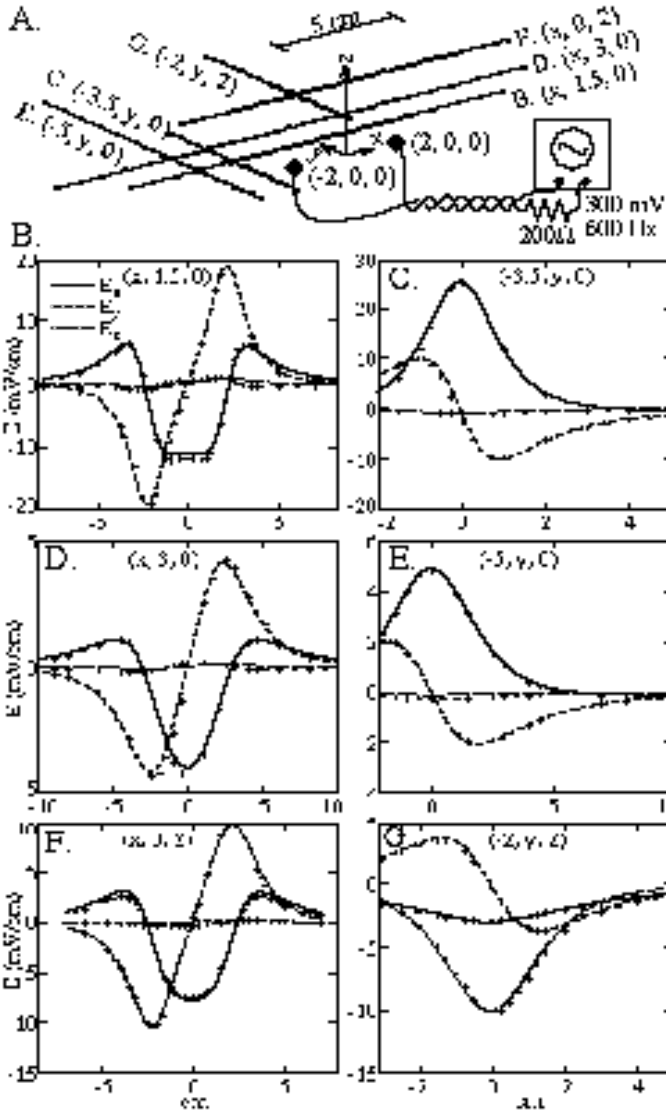

Fig. 1. A. The electric field was measured and computed at points (dots) along 6 lines (**B-G**) near a dipole centered in the fish tank (coordinates are in cm). **B-G**. Comparisons between the theoretical and measured electric field. The theoretical field components (curves) were computed using Eqn. 3 and measurements of the water conductivity and function generator current. The measured field components ('+') were computed using differential potential measurements from the array and Eqns. 1 and 4. **B-D** are in the same horizontal plane as the dipole, **F** is 2 cm above both poles, and **G** is 2 cm above one pole and perpendicular to F. Optimization of the interelectrode distance matrix (Eqn. 4) makes possible this level of accuracy.

$$\mathbf{E}(\mathbf{x}) = \frac{\rho I}{4\pi}\left(\frac{\mathbf{x}-\mathbf{x}_1}{|\mathbf{x}-\mathbf{x}_1|^3} - \frac{\mathbf{x}-\mathbf{x}_2}{|\mathbf{x}-\mathbf{x}_2|^3} \right) . \qquad (3)$$

Since the field decays with distance faster than the potential, the vertical water surfaces had smaller effects, and were ignored. The array used in the experiments presented here had interelectrode spacings matrix (Eqn. 1, in mm) of:

$$\begin{bmatrix} 2.203 \pm 0.014 & 0.264 \pm 0.003 & 0.177 \pm 0.022 \\ 0.452 \pm 0.006 & 1.315 \pm 0.000 & -0.038 \pm 0.002 \\ 0.290 \pm 0.015 & 0.053 \pm 0.068 & -1.231 \pm 0.034 \end{bmatrix} \qquad (4)$$

where the uncertainty is the standard deviation from two independent calibrations (average standard deviation is 18 μm). The fields computed from Eqn. 3, and Eqns. 1 and 4 are compared in Fig. 1.

Data analysis. From the digitized time series, an integral number of EOD periods nearest to one or two periods of 60 Hz was Fourier transformed. Transforming an integral number of periods minimizes aliasing errors and the need for windowing the data (Bloomfield 1976). Because *Apteronotus* has an extremely stable and band-limited EOD (Fig. 2 and Rasnow et al. 1993) the waveform can be accurately reconstructed from the complex amplitudes (or real amplitudes and phases) of its fundamental and lowest several harmonics. The amplitudes of the first 10 harmonics were computed by convolving the time series with precomputed sine and cosine series for each harmonic (the classical Fourier transform). This calculation is considerably faster than the Fast Fourier Transform, which computes amplitudes of all frequencies.

Delta-sigma ADCs sample continuously and asynchronously with respect to the EOD, therefore the phases of successive records were only aligned within one sample, or 21 μsec of each other. Additional synchronization was achieved computationally by shifting phases of the Fourier data so that the fundamental on the phase reference channel were exactly aligned (Rasnow 1994). We define zero phase as the positive-slope zero crossing of the EOD fundamental recorded between the reference electrodes. All the data shown below are aligned with this phase of the EOD.

Results

We present here several different views and representations of the 3-dimensional electric field vector generated by *Apteronotus leptorhynchus*, as it varies in both space and time around the fish. Along certain geometrical lines or planes, a field component may be weak, due to symmetry of the body and electric organ (Figs. 4 and 5), permitting a dimensional reduction (Figs. 8 and 9). In addition, the time variation can be eliminated by replacing the waveforms at each location with amplitude and phase functions computed by the Fourier transform (Figs. 2 and 6). Since the harmonic amplitudes decrease rapidly with increasing order, the complicated waveforms at any point can be accurately described with fewer than 10 complex numbers (Fig. 2).

EOD stability

The stability of the EOD waveform is fundamental to our method of generating the field maps. We analyzed the

variance of the EOD potential recorded between stationary reference electrodes during 25 minutes of mapping (Fig. 2A, inset). The standard deviation at every phase was less than 0.003 times the peak-to-peak amplitude. In the frequency domain, the coefficient of variation (standard deviation/mean) of the fundamental, second harmonic (twice the fundamental), and third harmonic amplitudes were 0.0051, 0.0052, and 0.0090 (Fig. 2B). The higher harmonics had lower amplitude and lower amplitude variance. The variance was ultimately limited by measurement noise.

Since individual waveforms were aligned by equating the phases of the fundamental, the standard deviation of the fundamental phase is, by construction, zero. The phases of the second through fourth harmonics, relative to the fundamental, varied within 0.2, 0.3, and 0.7 degrees (standard deviation) over the 25 minute recording period (Fig. 2C). These harmonics have frequencies of approximately 1.6, 2.4, and 3.2 kHz respectively. Changing units from frequency to time, these phase variations correspond to temporal jitter of 340, 360, and 620 nanoseconds respectively (Fig. 2D). We also observed similar stability at other locations in the near field. All the fish we studied had ≤ 1 μsec of phase jitter in their lowest harmonics.

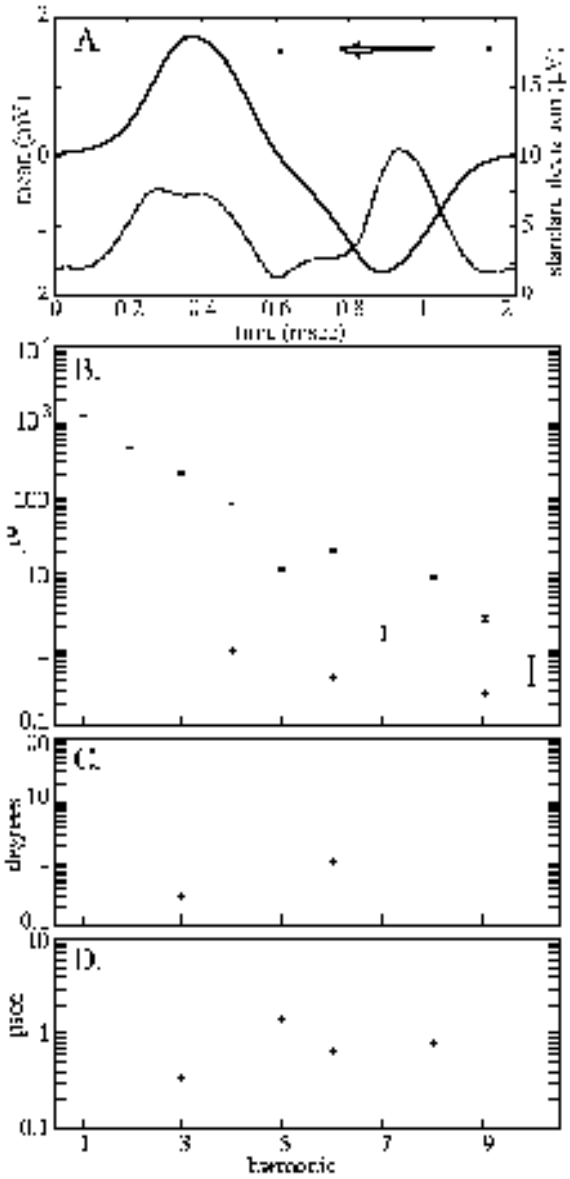

Fig. 2. While mapping the field in a plane, the waveform between two electrodes rostral and caudal of the fish (inset, **A**) was recorded as a phase reference. The waveform in **A** (solid line) is the average of 755 such measurements taken at approximately 2 second intervals during 25 minutes. The standard deviation at 100 discrete phases are shown by vertical errorbars (which are generally less than the line width of the waveform, and are thus invisible), and by the broken line with scale on the right. **B** Mean (upper) of the harmonic amplitudes. The standard deviation is shown by both errorbars on the mean values, and the lower dots. **C**, **D** Standard deviation of the relative phase of each harmonic for the same measurements. By construction, the standard deviation of the fundamental phase is zero.

Electric field components

We have decomposed the electric field vector into three Cartesian components in directions rostral (E_r), lateral (E_l), and dorsal (E_d), relative to the fish. Our first goal was to investigate how the field and potential waveforms varied along the body. In the approximate midplane, the potential and lateral field amplitudes at the tail were 15 and 80 times larger than at the head. Because of this large dynamic range, we had to normalize the waveform amplitudes in Fig. 3. Over most of the trunk, the lateral field component is largest, and is similar in waveform to the potential. At the head, all electric field components have similar waveforms and phases as the potential. Likewise, at the tip of the tail and in front and behind the fish, the field and potential waveforms have similar shape, except for opposite signs of some field components. For example, behind the tail and during the first half of the EOD cycle, the potential is strongly negative and the tail is sinking current. Caudal of the sink, the current flows in a rostral direction ($E_r > 0$) and towards the fish ($E_l < 0$). Between the trunk and tail, the waveforms change dramatically with rostrocaudal position.

The EOD slope or slew rate is largest in the narrow part of the tail. Also at the tail and behind it, the plateau near zero amplitude has longer duration than at the head. This is the result of superposition of the EOD harmonics, which also affect the number of peaks in the EOD waveforms. Over much of the caudal body, the potential and electric field have large harmonic components. Spectral analysis of the EOD is discussed further below.

We can visualize the dynamics of the field in two spatial dimensions by representing the instantaneous EOD amplitudes in grayscale (Fig. 4). Lateral of the fish, the lateral field component is largest and most spatially similar to the potential. A rostral-to-caudal propagation of peaks is evident in the caudal half of the fish. The rostral trunk, in contrast, is more uniform at any particular time,

and only near the zero-crossings does E_l have different

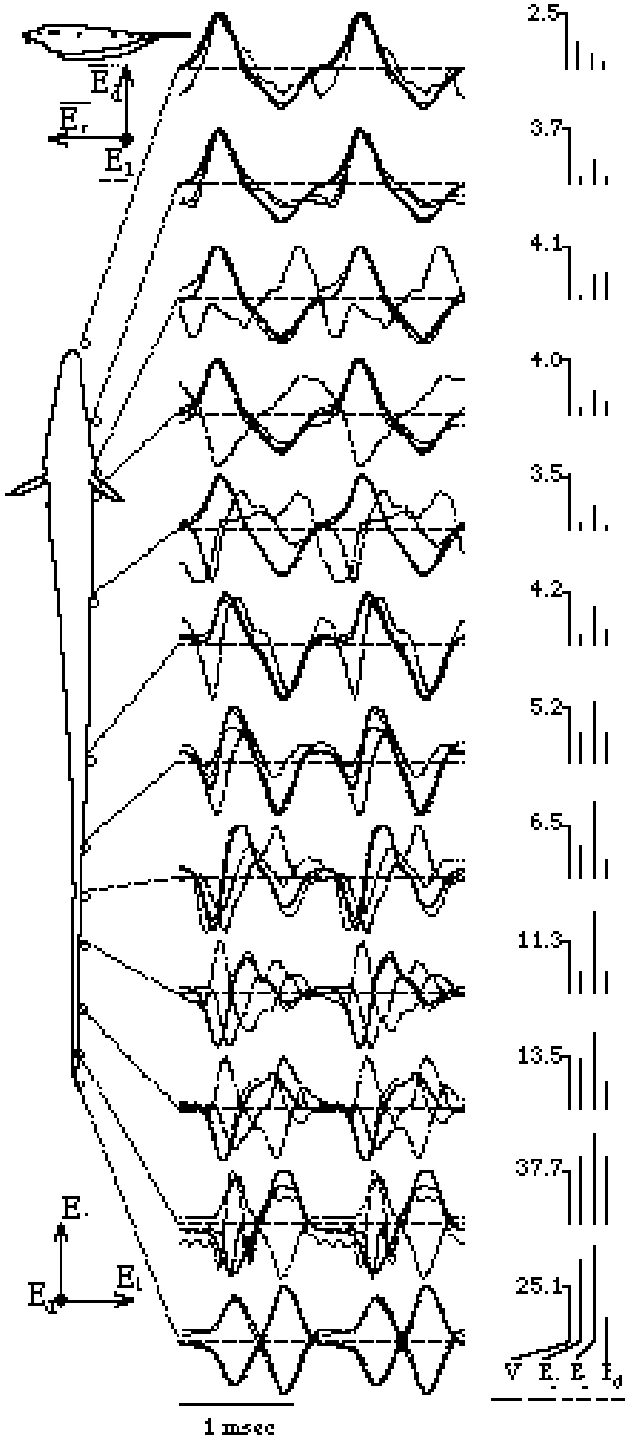

Fig. 3. Two periods of the electric potential (solid lines) and three electric field components, directed rostral, lateral, and dorsal (broken lines) are shown at points on the surface of *A. leptorhynchus*. Each waveform is normalized because of the large dynamic range. The actual amplitudes are indicated by the bars and scales on the right (potential units are mV and the field units are mV/cm). Although the potential and field components are in phase with each other at the head, the waveforms and phase relations become complicated caudal of the operculum.

signs at different locations along the trunk. The locations of the minima of the lateral electric field component (E_l) coincide with minima in the potential map, and peaks in the rostral field (E_r). This is consistent with current flowing from sources at the E_l peaks to sinks at E_l minima. The sign of E_r changes near the operculum, where the rostral component of the normal vector to the body also changes sign. The dorsal field component in the midplane is small, as expected by symmetry of the body and electric organ.

The potential and field in the dorsoventral plane and on the lateral body surface are shown in Fig. 5. Due to symmetry, the lateral component is small, except where measured on the body surface, off the symmetry plane. The dorsal component has opposite signs above and below the fish, consistent with the sign of this component of the vector normal to the body. The head, and in particular, the mouth, is a relatively strong field source (this is less apparent, but also visible in the midplane, Fig. 4). Generally, the rostral field component is similar in the two planes. The dorsal component in the dorsal plane is similar to the midplane lateral component, indicating that the field is approximately radially symmetric.

Spectral analysis

A great deal of information about the EOD dynamics can be obtained from spectral analysis. The majority of the temporal dynamics is contained in the amplitudes and phases of the lowest few harmonics, which are shown in Fig. 6. Over the head and trunk, the fundamental has relatively constant amplitude and phase, and dominates the EOD. The second and third harmonics near the head and tail are approximately 180° out of phase with the fundamental, which causes the plateau at the initial and final phases of the EOD waveforms, and stepens the slope between peaks (Fig. 3). Approximately 30 percent caudal of the mouth, the second harmonic gradually increases in amplitude and decreases in phase. This corresponds, in the time domain, to the rostral-to-caudal propagation of the EOD peaks, which is greatest caudally, where the harmonics are largest relative to the fundamental. Around 70 percent caudal of the mouth, the fundamental amplitude drops and changes polarity (180 degree phase change). In this area, both the second and third harmonics exceed the fundamental amplitude, resulting in complex waveforms with multiple zero crossings per EOD period.

The lateral electric field component in the midplane, and dorsal electric field component measured in the dorsal and ventral planes (Fig. 6, row 2) correspond approximately to the component of current flowing radially from the fish. These field components show similar amplitude and phase patterns as the potential. A notable difference is in the caudal part of the fish, where the second harmonic has comparable or greater magnitude as the fundamental. In front of and behind the fish, the field vector is dominated by the rostral component (Fig. 6, row 3), which also has a large second harmonic.

By symmetry, we expect the dorsal electric field component in the midplane and the lateral field

component in the dorsal and ventral planes to be small (Fig. 6, row 4). The only deviation from this is the midplane dorsal component, which has a large peak at the location of the pectoral fin. The lateral and rostral fields have local minima at the same place, suggesting that the pectoral fin is directing current dorsal and parallel with the fin surface.

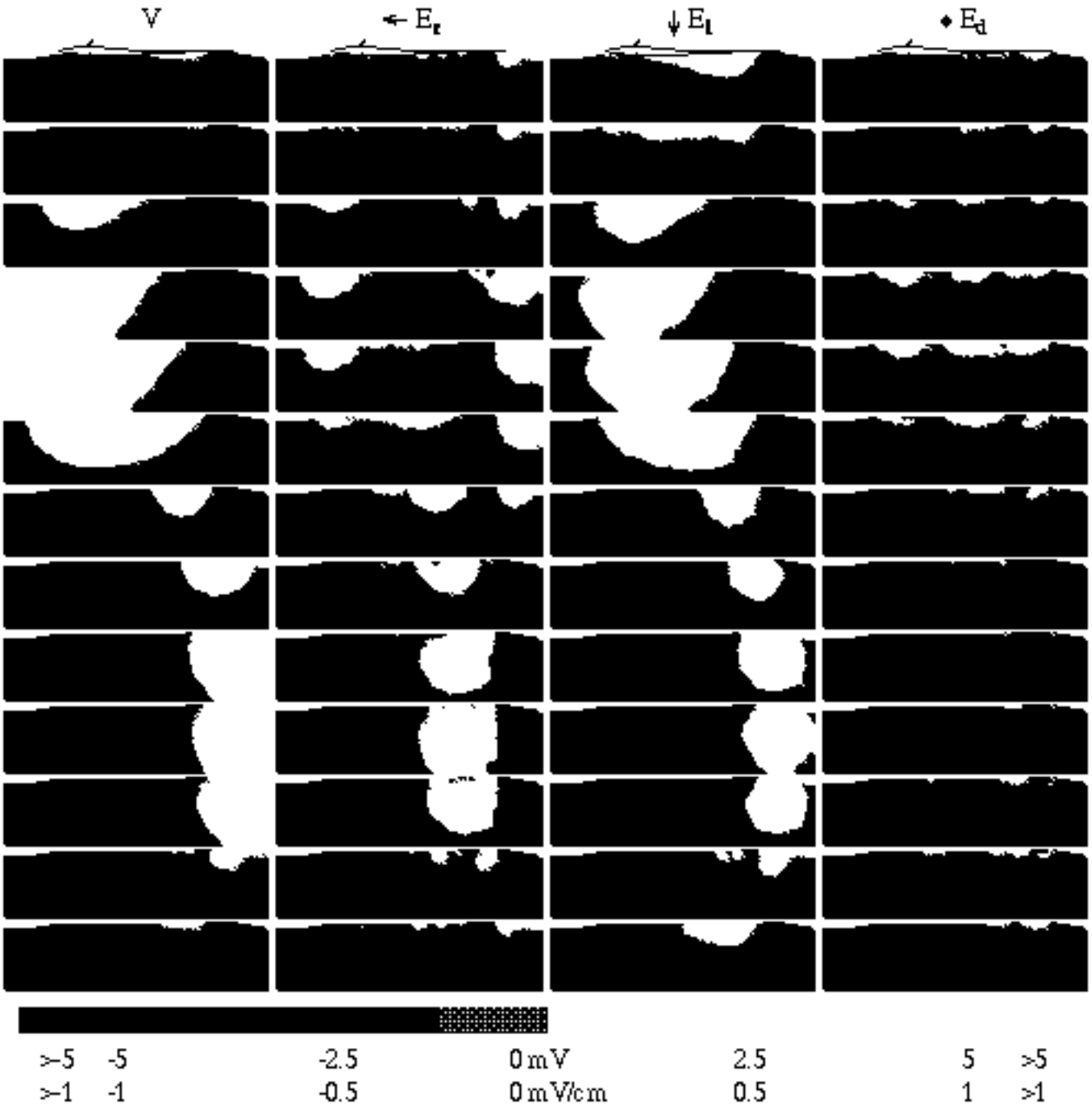

Fig. 4. Grayscale representation of the potential and field at 13 successive 100 μsec intervals constituting one EOD period. Black and white represent potentials and fields less than –5 mV and –2 mV/cm, and 5 mV and 2 mV/cm respectively (the peaks are clipped). The top frames are synchronous with the positive slope zero crossing of the potential fundamental measured in the far field from head to tail. The dorsal field is much weaker than the other field components in the midplane because of symmetry.

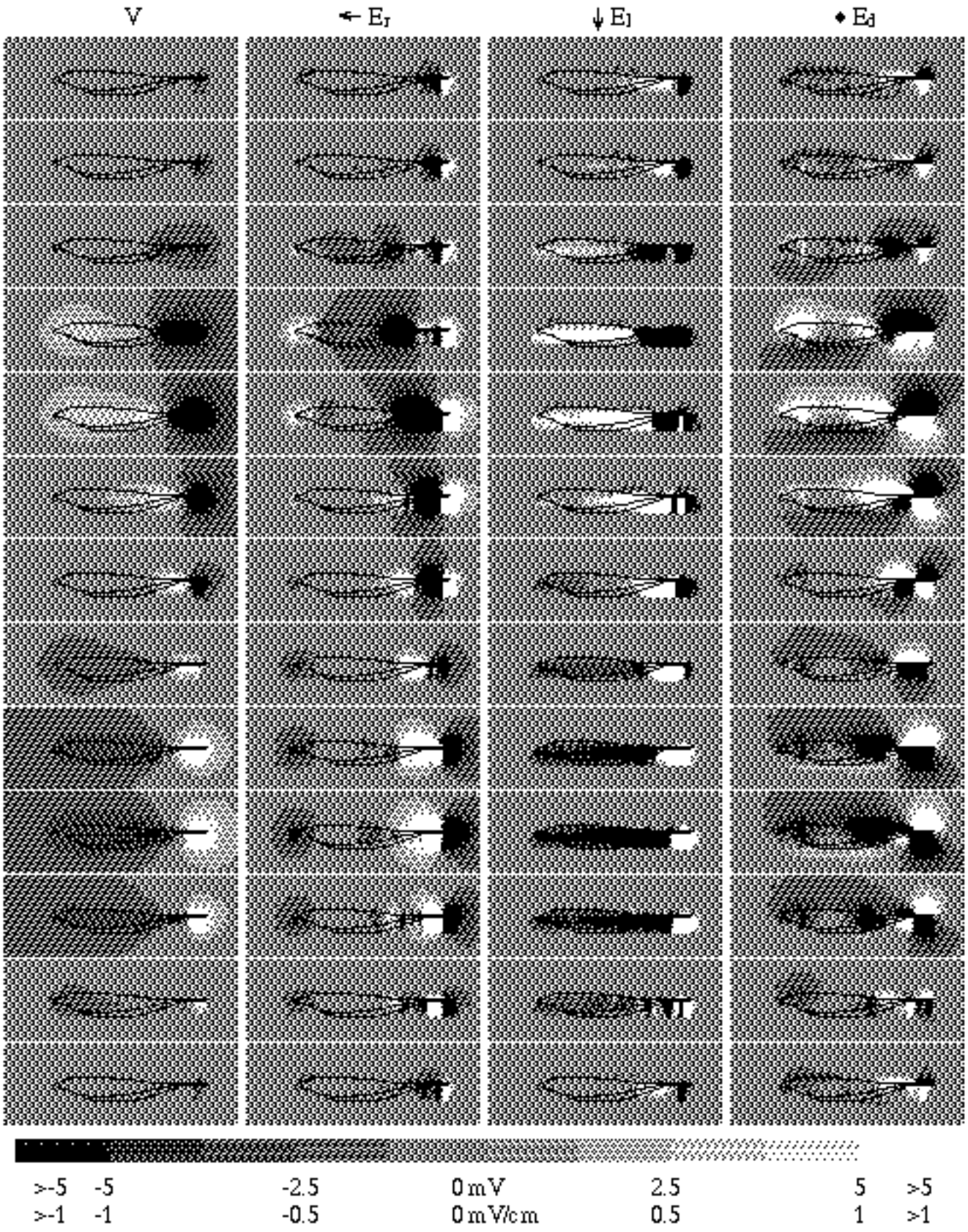

Fig. 5. Same as Fig. 4 but in the dorsoventral plane. The potential and field were not measured immediately under the chin or tail, resulting in some interpolation artifacts in these regions. The lateral field component is weak due to symmetry, except on the body, where the measurements are on the skin, and thus are lateral of the midline.

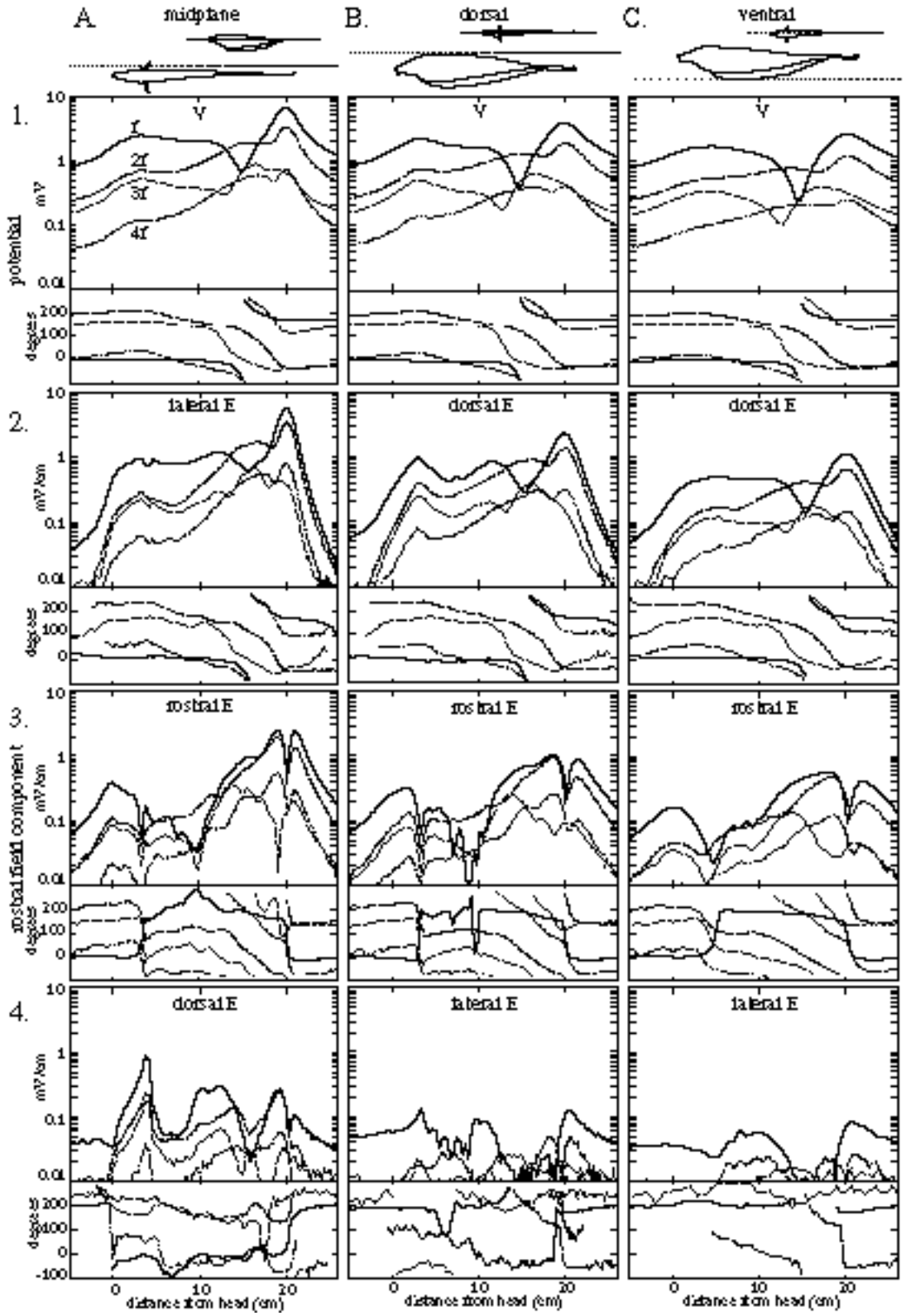

Fig. 6. Spectral analysis of the EOD in the midplane (column 1), above the back (column 2), and below the ventral fin (column 3). The recording sites are shown from two perspectives at the top of each column. The rows show the amplitudes and phase angles of the fundamental and lowest three harmonics of the potential (row 1), and the rostral, lateral, and dorsal electric field components (rows 2-4). Phases for amplitudes less than approximately 5 μV/cm are uncertain and are not shown. The potential and field are largest at the tail. Harmonics are weakest on the trunk, but account for a considerable amount of the EOD amplitude near the tail. Rostrocaudal propagation corresponds to the gradual caudal decrease of harmonic phase.

Lateral attenuation

The electric potential and field do not attenuate with distance from the fish at a constant rate (Fig. 7). Adjacent to the fish, the potential and field attenuate more gradually than 1/r (Fig. 7 B). Further lateral, the field decays approximately as 1/r at the head and $1/r^2$ lateral of the tail (Fig. 7 D). These are the decay rates for a line charge and point charge respectively. Note that these exponents critically depend on the choice of origin, and would be different had the least-squares-fit been applied to the magnitude vs. distance from the skin. The centerline was chosen for the origin of the distance scale because it is the axis of symmetry of the field.

The electric field vector

Neglecting the relatively small dorsal electric field component in the midplane, we can combine the other field components, (E_r, E_l), into 2-dimensional vectors (Fig. 8A). Likewise, in the dorsoventral plane, the lateral component is generally weak, and the field can be approximated by 2-dimensional vectors, (E_r, E_d), (Fig. 8B). In both planes, two peaks are stationary in space: one at the gill area and the other 0.5-1.0 cm rostral of the tail tip. Elsewhere, local peaks move with changes in EOD phase. Where the second harmonic is larger than the fundamental (from Fig. 6), the field changes direction twice per EOD cycle. For example, around 40 percent (9 cm) caudal of the mouth, the field vector oscillates rostral and caudal twice per cycle. Likewise, E_l changes sign twice per cycle 70 percent (15 cm) caudal of the mouth.

A notable feature of Fig. 8 is that the field vectors in the caudal part of the body change magnitude and direction whereas rostral of the operculum, only the magnitudes and sign, but not the direction, change significantly during the EOD cycle. This is also true away from the body (Fig. 9). Each curve in Fig. 9 shows how the electric field vector at a point in space changes direction and relative magnitude as it evolves through the EOD cycle. In front of the pectoral fin, the rostral and lateral (Fig. 9A; rostral and dorsal in Fig. 9B) field components have the same phase throughout the EOD cycle. Elsewhere, due to harmonics, the two field components are in phase with each other only during part of the cycle. During the first half of the EOD cycle, the field vectors above the middle third of the body sweep counter-clockwise and outward. In the second half of the EOD, the field is directed approximately normal

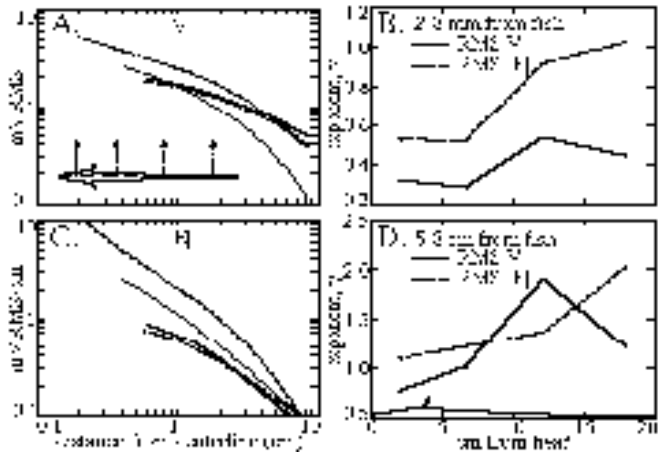

Fig. 7. The RMS potential (**A**) and electric field magnitudes (**C**) are shown as a function of distance from the centerline (the rostrocaudal axis in the midplane). The attenuation rate increases with distance from the fish. Fitting sections of these graphs to a power law: $y \propto x^{-\gamma}$, for distances between 2 and 8 mm (**B**) and 5–8 cm (**D**) from the skin, shows the power, γ, increases from head to tail. The potential attenuates fastest near the null of the dipole.

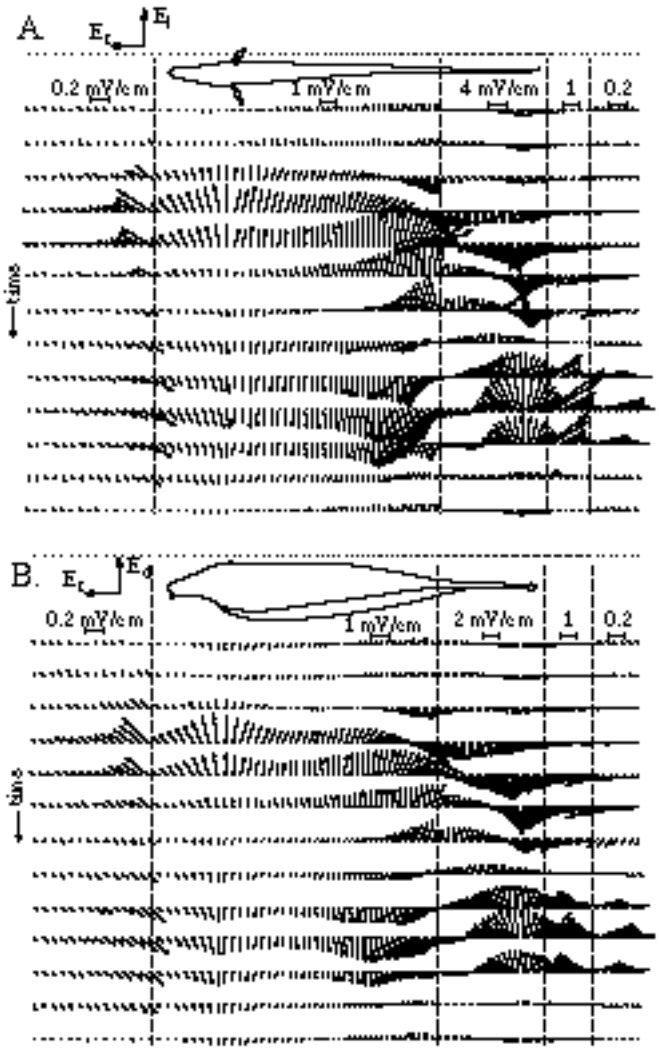

Fig. 8. A One cycle of the EOD measured along a line (top row) near the fish. At each point, the rostral and lateral field components form 2-dimensional vectors, which are shown at the same 13 phases of the EOD cycle as in Figs. 3 and 4. The vectors have been scaled by 0.2 and 0.05 on the body and tail regions (vertical dotted lines) to accommodate the large dynamic range. **B** Analogous view of the (E_r, E_d) field components, measured above the dorsal midline . Radial symmetry is evident.

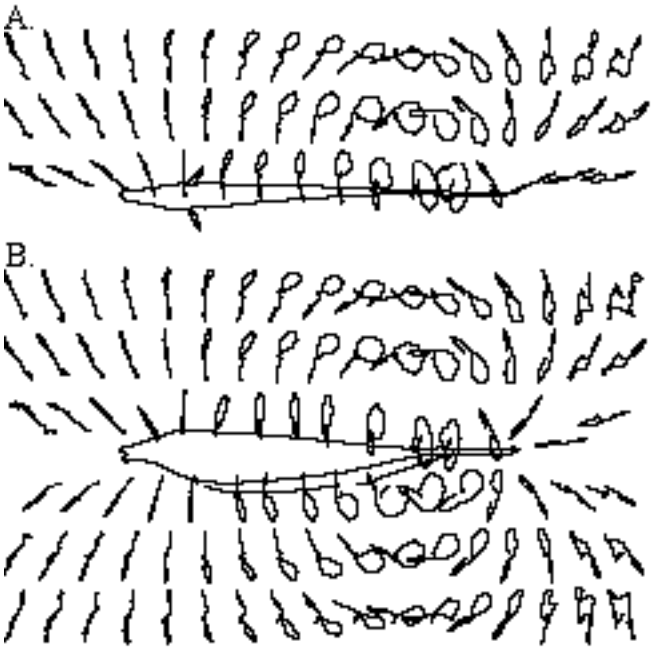

Fig. 9. Another time domain representation of the EOD cycle, showing the direction of the electric field vector at several points in the midplane. At each point, the initial EOD phase is drawn as a vector, and for subsequent times, just the tip of each vector is traced. The last phases were omitted to orient the curves. The peak magnitudes have also been normalized at each point (thus the curves far from the fish show more noise). Above the middle third of the body, the field angle rotates counterclockwise during the first half of the EOD cycle. In contrast, there is little rotation rostral of the operculum and behind the tail.

to the fish, and oscillates in amplitude without significant rotation.

Variation between fish

All the data presented here are from a single *A. leptorhynchus*. Similar measurements were made on two other *A. leptorhynchus*, and two *A. albifrons*. The major features of the EOD shown here were seen in all fish. Specifically, when normalized for frequency shifts, the EOD waveform was extraordinarily stable with time. Higher slew rates were observed caudally, and the EOD showed a rostral-to-caudal propagation at the tail. The EOD amplitude peaked slightly at the gill, and strongly near the tip of the tail. The second harmonic always exceeded the fundamental where the phase of the fundamental abruptly shifts. Caudal of this point, the second harmonic remained larger relative to the fundamental than in the rostral region of the fish. The rotation of the field vector in the caudal body and tail (Fig. 9) was strikingly similar in all fish.

The major differences between individual fish were EOD frequency, absolute amplitude, and the precise locations and detailed pattern of propagation of field peaks (Rasnow et al. 1993). For example, in one *A. albifrons*, the electric field only rotated over the caudal half of the body, but in most of the fish, the rotation was notable over 2/3 of the body caudal of the pectoral fin. Some fish also had two peaks of the fundamental at the tail. The more rostral fundamental peak, located around 80 percent from the mouth, where the body tapers and the ventral fin terminates, was in phase with the head and most of the trunk. This peak was several times smaller than the more caudal one, that was present in all fish. In spite of the differences in body plan between *A. leptorhynchus* and *A. albifrons*, we did not note any major differences in their respective EOD patterns.

Discussion

This study is a continuation of our work to thoroughly describe the electric organ discharge of *Apteronotus leptorhynchus*, with the goal of understanding how this and other species of electric fish may control and use their electric sensory-motor systems. Previously, we presented detailed maps of the electric potential, recorded relative to a distant reference electrode (Rasnow et al. 1993). We refer the reader to that paper for a general discussion. The electric field maps shown here support the findings of that study, and additionally reveal several EOD features not immediately apparent from the potential maps, such as the field's rotation (Fig. 9). The field maps also are the basis for quantitatively accurate simulations of the electric images of objects (Rasnow 1996).

Because the electric field of *Apteronotus* is a complicated function of position and its amplitude varies over several orders of magnitude around a fish, we have described it in terms of several parameters, e.g., spectral composition, field direction, and decay exponents. It is difficult to quantitatively compare many of these parameters in different fish because of their strong dependence on position around each fish. For example, Fig. 3 shows how waveforms change substantially over small regions of the body. Also, comparing the spectral composition of different regions of the fish (Fig. 6) is complicated by slight differences in the distances between the recording sites and the body. For these reasons, we found qualitative comparisons by visual examination of 2-dimensional maps (e.g., Figs. 4 and 5) a more useful approach. We have also assembled these maps for several fish as pseudocolor animations.† The basic properties of the electric field presented here were seen in all the fish that we have studied. Furthermore, the general similarities in the electric field among our small sample of *A. albifrons* and *A. leptorhynchus* suggests these two species have similar electric organ systems.

Observing the animations reveals how the electric field makes the transition from the complex multiphasic pattern near the fish to an approximately simple dipole further away. At times between the head-positive, tail-negative and head-negative, tail-positive dipolar phases, the spatial pattern of the potential becomes predominantly quadrapolar (head and tail positive, body negative, and visa-versa). The quadrapolar field attenuates more steeply with distance from

† The data and software to view these animations on color Macintosh computers are available on the internet computer network, by anonymous ftp at babel.bbb.caltech.edu; cd pub/ElectricFish.

the fish than the dipolar EOD phases. This results in a global null of the far field while the near field is nonzero. There is no time during the EOD cycle when the amplitude is synchronously zero everywhere, as would be the case for a simple oscillating dipole.

Since this is a descriptive study, it cannot by itself distinguish functional roles for the various EOD components and parameters. For example, some EOD components may be just incidental artifacts of controlling a long and fast electric organ, and serve no role in facilitating electric sense. However, it is likely that if a parameter is stable and contains useful information about the environment, then there could be a selective advantage for the fish to attend to it. Furthermore, it is well established that electric fish possess the necessary receptors and elements of the neural circuitry to encode and process amplitude, harmonics, timing and phase, and direction of electric fields (e.g., Hagiwara et al. 1965, Carr and Maler 1982, Nelson et al. 1993, Yager & Hopkins 1993).

The electric organ and fish interior

The neurogenic electric organ and its control circuitry in *Apteronotus* have been the subjects of numerous studies (see Bass 1986; Dye and Meyer 1986 for reviews). Knowing the electric field outside the fish cannot uniquely determine the internal distribution of sources and sinks. However, there are constraints on the continuity of the electric field, and estimates of the impedance of the fish that permit some conclusions about current flow to and from the electric organ (EO). In the water, the electric field and current are proportional, therefore the maps of the field are equivalent to maps of the current vector. These maps support our earlier conclusions (Rasnow et al. 1993) that the EO is not globally synchronous. In addition to showing a clear rostral-to-caudal propagation of the peaks and nulls of the electric field components, the electric field maps show that the direction of current flow changes over the EOD cycle in a complicated manner.

Bennett (1971a) proposed that the skin over the tail channels current to the body and tail tips, thereby increasing the dipole moment. However, Heiligenberg (1975) and Hoshimiya et al. (1980) found by simulations that the skin impedance at the tail must be low relative to the rest of the body, in order to balance the impedances of the small tail and the much larger body. Our data suggests both these principles operate to some extent. In contrast to the mouth and, more weakly, the gills, which act as approximately radial current sources and sinks (consistent with these areas being lower impedance paths to the body interior and EO), current emanates radially from different tail segments during different phases of the EOD. It is unlikely that this is due to low impedance pathways selectively channeling current through the skin, for these would somehow have to change with EOD phase. It is more probable that this pattern reflects sequential activity of the underlying segments of the EO. This implies that the skin at the tail does not severely impede the current from the underlying EO segments, as proposed by Bennett.

In some fish, the EOD amplitude had peaks at the base and tip of the tail. This suggests that some current channeling is occurring. However, based only on our data outside the fish, it cannot be determined whether this is due to the skin and/or other internal structures, such as the membranes surrounding the electric organ (Bennett 1971a). Additional leakage current through the skin between these peaks was always evident in all fish.

Boundary conditions require that the tangential component of the electric field is continuous at the interface between the skin and the water. Caudal of the gill, the tangential electric field is nonzero during certain phases of the EOD. Therefore there must be tangential currents within the skin. Although physically thin, the relatively high impedance of the skin confers it a large effect on the current flow from the EO. We have measured the impedance of excised skin patches on the trunk of another *Apteronotus* to be approximately 3 $k\Omega\text{-}cm^2$, and primarily ohmic (unpublished measurements, similar to Scheich and Bullock, 1974). It is therefore unlikely that the interior could be equipotential, which implies a normal electric field on the inside boundary of the skin, that is subsequently redirected within the skin. More likely, the body is not equipotential, and contains tangential currents as well. In support of this, we measured a bulk body impedance of 300 Ω-cm in the rostrocaudal direction (also consistent with Scheich and Bullock, 1974). We also measured in a live fish 0.5 mV RMS potential differences between internal electrodes separated by approximately 3 cm. The transdermal potential nearby was 0.7 mV RMS. Thus although the interior may be considered equipotential for certain analyses, it is important to recognize that this is only an approximation. Internal potential differences may complicate direct measurement of transdermal potentials. However, since one is often interested only in changes in transdermal potential (e.g., caused by a nearby object), a constant internal potential drop may not affect the difference.

Electroreceptors

Like other weakly electric fish, *Apteronotus* has two types of electroreceptors that detect its own EOD (Scheich and Bullock 1974). Amplitude and phase are encoded by P and T receptors respectively, although P units also encode phase (Bastian 1981; Scheich et al. 1973), and there is evidence that this rigid classification may be oversimplified (Viancour 1979). Although P-receptors in *Apteronotus* are primarily tuned to the EOD fundamental, they show a second tuning peak at the second harmonic (Hopkins 1976). Behavioral thresholds to external fields also show higher sensitivity to the second harmonic (Knudsen 1974). Furthermore, the receptors may respond in a nonlinear way to EOD spectral components (Fleishman 1992). In the caudal part of the fish, the second harmonic of the field is closer in amplitude to the fundamental than the corresponding spectral components of the potential. Therefore, the second harmonic may have even larger sensory significance than is suggested by the potential spectra.

The second and higher harmonics are generally of the appropriate phase to increase the slope or slew rate of the EOD. This could improve the temporal acuity of the T-receptors, which encode the timing of inward current zero-

crossings (Scheich et al. 1973). The positive and negative slope zero crossings are not symmetrical, and in much of the fish, have different slope (Fig. 3). The negative slope zero-crossing, which corresponds to the beginning of inward current flow, is the steepest phase of the EOD over most of the body, and would therefore be most immune to noise.

Unfortunately, T-units have not yet been adequately studied in *Apteronotus*, in part because they are relatively rare, constituting approximately 10 percent of the electroreceptors (Hopkins 1976). Fleishman (1992) claims that T-units in *Sternopygus* encode the positive slope zero crossing of the EOD. However, we suggest that this result may be erroneous due to their stimulus geometry. For these experiments, the fish's own EOD was silenced and an electric field was supplied with external electrodes. This reverses the direction of current flow through the skin, because the fish's interior is further from the current sources, and therefore at a lower absolute potential than the outside.

Yager and Hopkins (1993) and McKibben et al. (1993) recently showed that electroreceptors in *Brachyhypopomus* (formerly *Hypopomus*) are selective to the electric field direction. Behavioral studies had previously demonstrated that electric fish follow the direction of applied electric fields (Schluger and Hopkins 1987; Davis and Hopkins 1988). The direction of the electric field vector is therefore another parameter that, in addition to phase and amplitude, contains sensory information that the fish may attend to. Because the direction of the field changes with position and EOD phase (Fig. 9), it could conceivably help in resolving electric images that, based on amplitude information alone, might be ambiguous between different sets of object parameters. It is notable that many of the receptors in *Brachyhypopomus* preferred field directions that were not normal to the skin. Whether electroreceptors in *Apteronotus* have similar directional sensitivity, or polarity preferences is not yet known.

Signals from electroreceptors near the gill are contaminated with a large modulation associated with the fish's respiration (Rasnow et al. 1993). Our data suggests there is another self-modulation of the electric field in this body region due to the pectoral fin (Fig. 6A4). Electric fish apparently cope with this, for they have numerous electroreceptors in this region (Carr et al. 1982; Bennett 1971b). Montgomery and Bodznick (1993) have elaborated much of the neural circuitry involved in the suppression of ventilatory signals in the skate.

Electrolocation

The decay of the electric field with distance from the fish is a major determinant of the range of electrolocation (Fig. 7). We have shown that this attenuation does not follow a simple power law, which is not surprising given the complex and dynamic distribution of current sources and multipoles within the fish. The field decays slowly nearest the fish because the body acts as a 2-dimensional surface of current sources, and therefore the current only slightly diverges. Further away, the body and tail act approximately as line sources. Figure 7 provides an estimate of the length of these sources: 15 cm for the body and a few cm for the tail. At distances of the order of their lengths, the decay rate increases towards that of a point source (1/r for the potential and $1/r^2$ for the field). At distances comparable to the fish's length, the field is dipolar, and already too weak for small objects to be detectable (Knudsen 1975). The near field decays faster at the tail than at the trunk and head for a given distance from the fish because the tail is physically smaller. The potential attenuates fastest between the trunk and tail poles, where dipole effects first appear.

In our previous study of the *Apteronotus* potential, we proposed that there may be differences in the fish's perception of objects along its rostrocaudal axis (Rasnow et al. 1993). At the head, the electric field is most uniform in amplitude, phase, harmonic composition, and direction. Thus any inhomogeneous electrical structure of an object near the head would not be confounded with inhomogeneity in the field. Also the electric images would be more stable to relative motion between the object and fish. In addition, because the electric field is perpendicular to the skin, the electric images may have higher spatial resolution (see Rasnow 1996). Caudally, the field is stronger near the fish, more spatially variable, and attenuates more rapidly with distance. Therefore the electric image of an object would be strongly modulated by changes in distance and position, as would occur for example, as the fish bends its tail.

The rotating caudal field would almost certainly add spatiotemporal features to the electric images of objects. An object's induced dipole moment is proportional to the electric field vector, and will thus rotate at the same rate. However, nonspherical objects could have different dipole moments in different field orientations, qualitatively analogous to them casting different shadows in different orientations relative to the angle of illumination. Therefore, the fish may acquire multiple perspectives of an object with its rotating electric field (Rasnow 1996, Fig. 11).

There are additional factors that would tend to increase the complexity and spatiotemporal information content of images of caudal objects. A dielectric object's image could also be phase shifted, and therefore the instantaneous dipole moment of the perturbation could have different orientation than the field. For dielectrics, both the magnitude and phase of the perturbation field will be different for each harmonic, which could result in complex changes in the EOD waveform and its timing. The larger spatial gradient of the caudal electric field could also generate stronger multipole moments.

Which of the features of the electric field described here may be used by electric fish to identify object characteristics, and which may even confound object images, is still unknown. The rostrocaudal differences in the electric field suggest that there should also be rostrocaudal differences in the activity of electroreceptors and higher order neurons. Such differences, if indeed they are found, could provide clues about the functional roles of these electric field properties. It is especially difficult to infer additional significance to the rotating field without a better understanding of electroreceptor transfer functions, which may have their own directional asymmetries (Yager and Hopkins 1993). We hope this description of the electric field will stimulate additional research in these directions.

Communication and interactions with other electric fish

In addition to passive object detection, electric fish identify and communicate with each other using their electric sense (Hopkins 1974; McGreggor and Westby 1992). Two approaching fish will initially interact by detecting the superposition of their own EOD with the far field of the other. Not only is the other fish's far field much weaker, but it is also more spatially uniform, and contains fewer harmonics than the receiver's near field. Since two fish generally have different frequency EODs, the perturbation amplitude will oscillate at the beat or difference frequency (Heiligenberg 1991). In contrast, the perturbations from passive objects will predominantly have the same spectral composition as the fish's own EOD.

In the wild, many of the interactions between electric fish are of a predatory nature or in defense of territory (Westby 1988). Both families of weakly electric pulse fish have been shown to approach other electric sources by swimming parallel to the electric field lines (Davis and Hopkins 1988; Schluger and Hopkins 1987). The fish rely primarily on the direction of the field, and not its amplitude, to find the source. It is interesting to speculate if the rotating field vector in the caudal body might benefit *Apteronotus* by confusing an electroreceptive predator attempting to follow its field lines. It is possible that upon entering the complex near field, a predator might pause or makes an abrupt correction to its trajectory. Such movements could be detected by the lateral line sense, and trigger an escape response.

Acknowledgments. We thank Chris Assad for his thoughtful comments and numerous personal and scientific contributions to this work. We are especially grateful, and wish to dedicate this paper in remembrance of Walter Heiligenberg, who's encouragement and perspective are dearly missed. This work was funded in part by NSF IBN-9319968.

References

Assad C, Rasnow B, Bower JM (1993) Numerical simulations of the electric organ discharge of weakly electric fish. In Eeckman FH and Bower JM, Computation and Neural Systems, Kluwer Academic Publishers, pp 281-286.

Bass AH (1986) Electric organs revisited: evolution of a vertebrate communication and orientation organ. In Bullock T.H. and Heiligenberg W. (Eds.) Electroreception. Wiley & Sons Inc., pp 13-70.

Bastian J (1981) Electrolocation I. How the electroreceptors of *Apteronotus albifrons* code for moving objects and other electrical stimuli. J Comp Physiol 144:465-479.

Bennett MVL (1971a) Electric organs. In: Hoar WS and Randall DH (eds) Fish Physiology. Academic Press, pp 347-491.

Bennett MVL (1971b) Electroreception. In: Hoar WS and Randall DH (eds) Fish Physiology. Academic Press, pp 493-574.

Bloomfield P (1976) Fourier analysis of time series: an introduction. John Wiley & Sons.

Carr CE, Maler L, Sas E (1982) Peripheral organization and central projections of the electrosensory nerves in gymnotiform fish. J Comp Neurol 211:139-153.

Carr CE and Maler L (1988) Electroreception in gyymnotiform fish: central anatomy and physiology. In Bullock T.H. and Heiligenberg W. (Eds.) Electroreception. Wiley & Sons Inc., pp 319-374.

Davis EA and Hopkins CD (1988) Behavioral analysis of electric signal localization in the electric fish *Gymnotus carapo* (Gymnotiformes). Anim Behav 36:1658-1671.

Dennis JEJ and Woods DJ (1987) New computing environments: microcomputers in large-scale computing. SIAM 1987:116-122.

Dye JC and Meyer JH (1986) Central control of the electric organ discharge in weakly electric fish. In Bullock T.H. and Heiligenberg W. (Eds.) Electroreception. Wiley & Sons Inc., pp 71-102.

Fleishman LJ (1992) Communication in the weakly electric fish *Sternopygus marurus* I. The neural basis of conspecific EOD detection. J Comp Physiol 170:335-348.

Hagiwara S, Szabo T, Enger PS (1965) Electroreceptor mechanisms in a high frequency weakly electric fish *Sternarchus* [*Apteronotus*] *albifrons*. J Neurophys 28:784-799.

Heiligenberg W (1975) Theoretical and experimental approaches to spatial aspects of electrolocation. J Comp Physiol 103:247-272.

Heiligenberg W (1991) Neural nets in electric fish. MIT Press.

Hopkins CD (1974) Electric ccommunication in fish. Amer Sci 62:426-437.

Hopkins CD (1976) Stimulus filtering and electroreception: tuberous electroreceptors in three species of gymnotid fish. J Comp Physiol 111:171-207.

Horowitz P and Hill W (1989) The art of electronics. 2nd ed., Cambridge University Press.

Hoshimiya N, Shogen K, Matsuo T, Chichibu S (1980) The *Apteronotus* EOD field: waveform and EOD field simulation. J Comp Physiol 135:283-290.

Jackson JD (1975) Classical Electrodynamics. Wiley & Sons Inc.

Knudsen EI (1974) Behavioral thresholds to electric signals in high frequency electric fish. J Comp Physiol 91:333-353.

Knudsen E (1975) Spatial aspects of the electric fields generated by weakly electric fish. J Comp Physiol 99:103-118.

McKibben JR, Hopkins CD, Yager DD (1993) Directional sensitivity of tuberous electroreceptors: polarity preferences and frequency tuning. J Comp Physiol 173:415-424.

Montgomery JC and Bodznick D (1993) Hindbrain circuitry mediating common mode suppression of ventilatory reafference in the electrosensory system of the little skate *Raja erinacea*. J Exp Biol 183:203-215.

Nelson ME, Payne JR, Xu Z (1993) Modeling and simulation of primary electrosensory afferent response dynamics in the weakly electric fish *Apteronotus leptorhynchus*. J Comp Physiol 173:746.

Rasnow B, Assad C, Nelson ME, Bower JM (1989) Simulation and measurement of the electric fields generated by weakly electric fish. in Touretzky DS (Ed) Advances in neural information processing systems 1. Morgan Kaufmann, pp 436-443.

Rasnow B (1996) The effects of simple objects on the electric field of *Apteronotus*. J Comp Physiol. (submitted).

Rasnow B (1994) The electric field of a weakly electric fish. Ph. D. Thesis, California Institute of Technology, University Microfilms.

Rasnow B, Assad C, and Bower JM (1993) Phase and amplitude maps of the electric organ discharge of the weakly electric fish *Apteronotus leptorhynchus*. J Comp Physiol 172:481-491.

Robinson DA (1968) The electrical properties of metal microelectrodes. Proc. IEEE 56:1065-1071.

Scheich H, Bullock TH, Hamstra RH (1973) Coding properties of two classes of afferent nerve fibers: high-frequency electroreceptors in the electric fish *Eigenmannia*. J Neurophys 36:39-60.

Scheich H and Bullock TH (1974) The detection of electric fields from electric organs. In Fessard A (Ed) Handbook of sensory physiology. Springer-Verlag, pp 201-256.

Schluger JH and Hopkins CD (1987) Electric fish approach stationary signal sources by following electric current lines. J Exp Biol 130:359-367.

Viancour TA (1979) Electroreceptors of a weakly electric fish. I. Characterization of tuberous receptor organ tuning. J Comp Physiol 133:317-325.

Welland DR, Del Signor BP, Swanson EJ, Tanaka T, Hamashita K, Hara S, Takasuka K (1989) A stereo 16-bit delta-sigma A/D converter for digital audio. J Audio Engr Soc, 37: No. 6.

Westby GWM (1988) The ecology, discharge diversity, and predatory behavior of gymnotiforme electric fish in the costal streams of French Guiana. Behav Ecol Sociobiol 22:341-354.

Yager DD and Hopkins CD (1993) Directional characteristics of tuberous electroreceptors in the weakly electric fish *Hypopomus* (Gymnotifromes) J Comp Physiol 173:401-414.